Nanoscale Research Letters

NANO EXPRESS Open Access

Effect of non-stoichiometry of initial reagents on morphological and structural properties of perovskites $CH_3NH_3PbI_3$

Anatolii Belous[1], Sofiia Kobylianska[1], Oleg V'yunov[1*], Pavlo Torchyniuk[1], Volodymyr Yukhymchuk[2] and Oleksandr Hreshchuk[2]

Abstract

The properties of films of organic-inorganic perovskites $CH_3NH_3PbI_{2.98}Cl_{0.02}$ depending on the ratio of starting reagents in solutions (PbI_2:{$CH_3NH_3I + CH_3NH_3Cl$}) has been investigated. It was found that the formation of the perovskite structure with the ratio of the initial reagents PbI_2: CH_3NH_3I = 1:1 occurs at 70–80 °C, and with the increase of the temperature of thermal treatment to 120 °C, the thermal destruction of the perovskite begins. When the ratio of the starting reagents PbI_2: CH_3NH_3I = 1:2, the formation of the perovskite structure occurs through the intermediate compound $(CH_3NH_3)_2PbI_4$, and when the ratio is 1:3—$(CH_3NH_3)_3PbI_5$ and $(CH_3NH_3)_2PbI_4$. Independent on the ratio of the initial components (CH_3NH_3I:PbI_2), the ratio between the content of lead and iodine in the films remains unchanged, that is why a significant difference in the film properties could be explained by the anisotropy of the particle shape, which is consistent with the data of electron microscopy and X-ray diffractometry.

Keywords: Metal halide perovskite, Film, Microstructure, Chemical reaction, Raman spectroscopy

PACS: 81.07.Pr, 81.07.–b, 81.70.Jb, 87.64.kp

Background

Nowadays, solar energy is emerging as alternate sources of energy and the development of technologies to transform renewable energy into electricity is essential to societal advancement [1]. The most widely commercialized solar cells based on crystalline or multicrystalline silicon and semiconductor CuIn, $GaSe_{2-x}S_x$, CdTe [2]. In practice, the most solar cells are based on silicon (85–90%) [3]. The theoretical power conversion efficiencies (PCE) of these solar modules are as high as 28–19.9%. However, for commercialized solar modules, PCE is only 18% for crystalline silicon solar cells and 12–14% for polycrystalline Si. The main disadvantage of silicon and semiconductor's based solar cells is the narrow spectral range of sensitivity to solar radiation and their indirect bandgap [4]. This causes the use of a large thickness (~ 100 μm) of the active layer to increase the amount of absorption of solar radiation and, consequently, leads to a relatively high cost.

Promising new class of solar cell is the perovskite one, which has drawn the considerable interest of the researchers due to a remarkable rapid growth of its PCE. Organic-inorganic perovskites (OIP) are a class of substances with typical chemical formula ABX_3, where A is an organic cation (often methylammonium $CH_3NH_3^+$, formamide $CH(NH_2)_2^+$), B is an inorganic cation (usually Pb^{2+}), and X is a halide anion (I^-, Cl^-or Br^-) [5, 6]. Synthesis of these compounds is relatively easy, and they have high photoelectric characteristics, in particular, the large diffusion length of charge carriers [7]. An impressive increase in PCE for solar cells based on OIP from ~ 3.4% in 2004 to 23.3% (22.6% certified) in early 2018 [8–10] has generated a considerable interest in the study of its properties. Significant achievements were obtained due to the development of novel technology for the formation of these compounds, which allow production of smooth and dense active layers of high-performance photovoltaic devices [11, 12]. The process of forming a smooth film without pores requires

* Correspondence: vyunov@ionc.kiev.ua
[1]V.I. Vernadskii Institute of General and Inorganic Chemistry of the NAS of Ukraine, Kyiv, Ukraine
Full list of author information is available at the end of the article

careful control of the chemistry of solutions of precursors and the conditions for their deposition [13–15]. In particular, deposition of a stoichiometric amount of methylammonium and lead iodides (MAI:PbI_2 = 1:1) on a glass substrate does not allow preparation of a dense film of methylammonium lead iodide perovskites ($MAPbI_3$), since in this case, the needle-like crystals grow. This film morphology significantly reduces the PCE. At the same time, using additional (super-stoichiometric) amount of MAI, a dense film can be prepared [16, 17].

Several fundamental properties make OIP extremely promising for photovoltaic applications, including low defect density, long charge carrier lifetime and diffusion length, low speed of recombination, and high optical absorption coefficient due to direct band gap [18, 19]. However, to date, many of the fundamental properties of OIP have not yet been studied in detail. It is known that one of the main drawbacks of this class of materials is their low stability. Exposure to even ambient atmospheric conditions causes severe degradation of OIP, and their unique optoelectronic properties diminish consequently. Numerous works have established the effects of moisture and oxygen, heat treatment at $T > 100$ °C, and the action of UV radiation ingress into $MAPbI_3$ films, and it is well understood that as MAI is evaporated, solid PbI_2 remains on the film [20–26]. This instability not only complicates the successful implementation of solar cells based on $MAPbI_3$, but also the study of the properties of this material. In particular, the X-ray diffraction analysis, Raman and photoluminescence (PL) studies with a large exposure time (> 6 s) leads to the destruction of the perovskite. Therefore, it is important to take into account these features in the study of OIP and to distinguish spectra of the materials and products of their decomposition under abovementioned factors. It should be noted that despite the degradation of this material under the influence of external factors, the number of works devoted to the study of its properties significantly increases each year [27–29]. This may indicate that the scientific community believes in the possibility of using perovskites in solar cells.

As noted above, the perovskite $MAPbI_3$ was extensively investigated by various methods, but today, there is little data on the influence of non-stoichiometric quantities of reagents on the properties of synthesized crystals. At the same time, the presence of various complexes (PbI^{3-}, PbI_4^{2-}) in the solution used for the synthesis of organic-inorganic perovskites affects the microstructure of the resulting film [30, 31]. In particular, the change in the ratio of CH_3NH_3I:PbI_2 from 1:1 to 1:3 in the initial solutions leads to significant changes in the microstructure and properties of the films [16, 32]. The investigation of the parameters of devices based on organic-inorganic perovskites $CH_3NH_3PbI_{3-x}Cl_x$ showed that with increasing MAI excess in the initial solution in the range from 1 to 3, values of open circuit voltage (Voc) increase, and the short circuit current density (Jsc), fill factor (FF), and power conversion efficiency (PCE) pass through a maximum at MAI excess of ~ 2–2.6 [33]. Therefore, the study of chemical and physical mechanisms, which, with non-stoichiometry of the starting reagents, significantly affect their morphological and structural properties, is very important both from the fundamental point of view and for the practical application of perovskites.

To study the influence of non-stoichiometry of the starting reagents on the properties of synthesized OIP, the Raman spectroscopy and X-ray diffractometry have been used. Raman spectroscopy is a sensitive and rapid method for diagnosing various compounds both in the form of solutions and in solids. Investigation of OIP by Raman spectroscopy and X-ray diffractometry methods can significantly expand the existing understanding of the processes of their formation, the features of the crystalline structure, and its effect on the film morphology.

In this paper, we aim to study the formation of films of organic-inorganic perovskite $CH_3NH_3PbI_{2.98}Cl_{0.02}$ and the influence of different ratios of the starting reagents (CH_3NH_3I: PbI_2) on their microstructure.

Methods

Methods of synthesis

Lead iodide (PbI_2), methylammonium chloride CH_3NH_3Cl, and pre-synthesized methylammonium iodide CH_3NH_3I were used as starting materials. To stabilize the perovskite structure, the partial substitution of iodine with chlorine was carried out by the addition of methylammonium chloride CH_3NH_3Cl [16, 34]. Dried dimethylformamide (DMF) was used as the solvent.

For the deposition of $CH_3NH_3PbI_{2.98}Cl_{0.02}$ films ($MAPbI_{3-x}Cl_x$), the starting reagents PbI_2, CH_3NH_3I, and CH_3NH_3Cl in ratios of 1:0.98:0.02 (hereinafter 1:1); 1:1.98:0.02 (1:2); 1:2.98:0.02 (1:3) was dissolved in DMF and stirred at 70 °C for 1 h. The films were deposited in a dry box. The previously obtained clear solution was deposited to the purified glass substrate and to the FTO (fluorine-doped tin oxide) substrates by spin-coating at 1200 rpm for 30 s. Thermal treatment of films was carried out on a preheated hot plate at temperatures from 70 to 180 °C for 30 min.

Characterization

The microstructure of starting reagents (PbI_2 i CH_3NH_3I) and OIP ($CH_3NH_3PbI_3$) was studied using a scanning electron microscope SEC miniSEM SNE 4500 MB. The elemental composition of the films was determined using an EDAX Element PV6500/00 F spectrometer, which is included in the set of this microscope.

The phase composition of films was identified by X-ray powder diffractometry (XRPD) using a DRON-4-07 diffractometer (CuKα-radiation, 40 kW, 18 mA) over 2Θ = 10–120°, a step of 0.04°, and a count time of 4 s. Structural parameters were determined by the Rietveld profile analysis method using XRPD data. Raman spectra were excited by 532 and 671 nm lines of solid state lasers and acquire usage of single stage monochromator equipped with charge-coupled device (CCD) detector (Andor). The exciting laser power was kept as low as possible, to avoid the damage of molecules under investigation either due to heating or photochemical reactions.

Results and discussion

Investigation of solutions

Figure 1 a, b show Raman spectra of pure DMF (curve 1) and dissolved compounds such as PbI_2 (curve 2), CH_3NH_3I (curve 3), PbI_2 and CH_3NH_3I in the ratio 1:1 (curve 4), PbI_2 and CH_3NH_3I in the ratio 1:2 (curve 5), PbI_2 and CH_3NH_3I in the ratio 1:3 (curve 6), and PbI_2 and CH_3NH_3Cl in the ratio 1:1 (curve 7) obtained by laser excitation at $\lambda = 532$ nm at room temperature. It should be noted that the solutions of both PbI_2 and CH_3NH_3I in DMF are practically transparent. At the simultaneous dissolution of PbI_2 and CH_3NH_3I in DMF the coloring of a solution changes from light yellow at a ratio of components (1:1) to a dark yellow (1:3). The coloring of the solution shows that there is a chemical interaction between the components of PbI_2 and CH_3NH_3I.

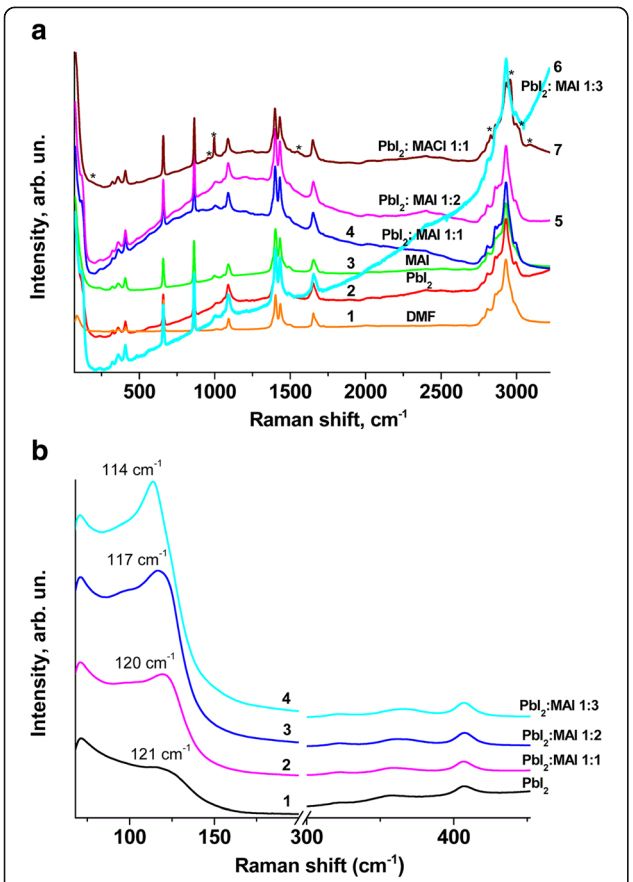

Fig. 1 **a** Raman spectra of a solvent DMF (curve 1) and dissolved in it compounds: 2 - PbI_2, 3 - CH_3NH_3I, 4 - PbI_2 and CH_3NH_3I (1:1), 5 - PbI_2 and CH_3NH_3I (1:2), 6 - PbI_2 and CH_3NH_3I (1:3), 7 - PbI_2 and CH_3NH_3Cl (1:1). **b** Raman spectra of solutions: 1- PbI_2, 2 - PbI_2 and CH_3NH_3I (1:1), 3 - PbI_2 and CH_3NH_3I (1:2), 4 - PbI_2 and CH_3NH_3I (1:3) in DMF in the low-frequency range. All spectra were obtained with $\lambda_{exc} = 532$ nm at room temperature

Sufficiently intense bands appear in the spectral region from 50 to 3500 cm^{-1} in the Raman spectrum of DMF (curve 1). Almost all the same bands occur in the spectrum of the solution of PbI_2 in DMF (curve 2), except one, which is a manifestation of the vibration mode of Pb-I with a frequency of ~ 114 cm^{-1} and some features in the region of 475 cm^{-1}. Only the Raman bands of DMF (curve 3) appear in the spectrum of the solution of CH_3NH_3I in DMF.

In the spectra of solutions in which both PbI_2 and CH_3NH_3I compounds were added in the ratio 1:1 and 1:2, except for bands with frequencies of 114 cm^{-1}, broad bands appear with maxima at 1000 and 1250 cm^{-1} (Fig. 1a, curves 4, 5), respectively. For the spectrum of the solution in which the PbI_2 and CH_3NH_3I compounds were added in the ratio of 1:3, the maximum shifts to a long-wave region (Fig. 1a, curve 6). It is most likely that all of them appear due to the contribution of photoluminescence from the formed compound $CH_3NH_3PbI_3$ because when the Raman spectra are excited with radiation $\lambda = 671$ nm, they do not appear in the spectra (spectra are shown in Additional file 1).

As noted above, characteristic Pb-I vibration band appears in the range 114–121 cm^{-1} (Fig. 1b) in all Raman spectra of solutions with different ratios of PbI_2 and CH_3NH_3I compounds. Its relative intensity increases and the maximum of the bands are shifted to the low-frequency side with an increase in CH_3NH_3I content in the solution (Fig. 1b). This shift of the Raman peak correlates with the shift of the optical absorption edge from 2.54 eV for PbI_2 in DMF down to 2.24 eV for the mixture of PbI_2 and CH_3NH_3I mixed in the ratio of 1:3 (spectra are added to the Additional file 1: Figures S1 and S2). These spectral changes indicate that adding of CH_3NH_3I increases the probability of forming lead polyiodides, such as $[PbI_3]^{-1}$, $[PbI_4]^{-2}$, $[PbI_5]^{-3}$, and $[PbI_6]^{-4}$. Our results correlate with the result of work [31], where the influence of precursors on the structural and optical properties of the perovskites was shown. The different composition of polyiodides can cause the different morphology of the perovskite films, including those observed in our work. Since a small fraction of CH_3NH_3Cl

(2% relative to CH_3NH_3I) was added to the solution together with CH_3NH_3I, it was necessary to establish the possible contribution of this compound to the Raman spectra. For this purpose, the Raman spectrum of CH_3NH_3Cl in DMF (Fig. 1a, curve 7) was registered. It shows a series of additional bands with the following frequencies: 178, 953, 997, 1547, 2829, 2957, 3020, and 3092 cm^{-1}, which in Fig. 1a, curve 7 are marked with asterisks. Indeed, these bands' frequencies are close to the frequencies of the Raman bands of the compound $CH_3NH_3PbICl_2$, obtained in [35]. However, the abovementioned bands are not manifested in the Raman spectra of $CH_3NH_3PbI_{2.98}Cl_{0.02}$ solutions due to a small fraction of chlorine atoms.

Investigation of films

Figure 2 shows images of the films of initial reagents deposited on the glass substrates surface.

The microstructure of CH_3NH_3I looks like glass with small heterogeneities of a certain shape on the surface (Fig. 2a). Microscopic and energy-dispersive X-ray spectroscopy (EDX) studies have shown that films are thinner in the area of heterogeneities BSE (backscattering electrons) analysis suggests that this is due to increasing the surface level in these places (see EDX spectra in Additional file 1). Such areas are probably formed due to the rapid evaporation of the solvent from the film. The significant increase in the number of such heterogeneities with temperature increase to 90 °C confirms this fact (Fig. 2b).

When PbI_2 solution is deposited at room temperature (without heating), large elongated (wire-like [36]) grains grow in all directions (Fig. 2c). At 90 °C, initially, the wire-like grains grow from a small number of crystallization centers. Further, the supersaturated solution is formed, and grains grow in supersaturated regime [37, 38] with the initially formed wire-like grains as seed particles (Fig. 2d).

Figure 3 shows the surface of the films of organic-inorganic perovskites that were deposited on the glass substrate and FTO/glass. When initial reagents (CH_3NH_3I:PbI_2) were taken in the ratio 1:1, the microstructure of the organic-inorganic perovskite film deposited on the glass substrate and FTO/glass practically does not differ: there are structured films with a significant anisotropy of the particle shape (needle-like). In the case of a ratio of initial reagents 1:2, particles in the form of a maple leaf are visible on the glass. The growth of the latter occurs from the center of crystallization in 5–6 directions. Between large particles, small leaf-like particles appear (see insert on Fig. 3b). At the same time, after deposition of the film on FTO/glass surface, particles become more isotropic in the form. This agreed with the data of Ref. [39], where a strong difference in microstructures is observed for films deposited on different polycrystalline and amorphous substrates. In the case of the ratio of initial reagents 1:3, the size of the particles is significantly reduced and a more dense film is formed.

Figure 4 shows the results of the XRPD analysis of films after heat treatment in the temperature range from 70 to 180 °C.

For the system with the ratio of the initial reagents PbI_2:CH_3NH_3I = 1:1, it was found that the single-phase product is formed at 70–80 °C by the reaction:

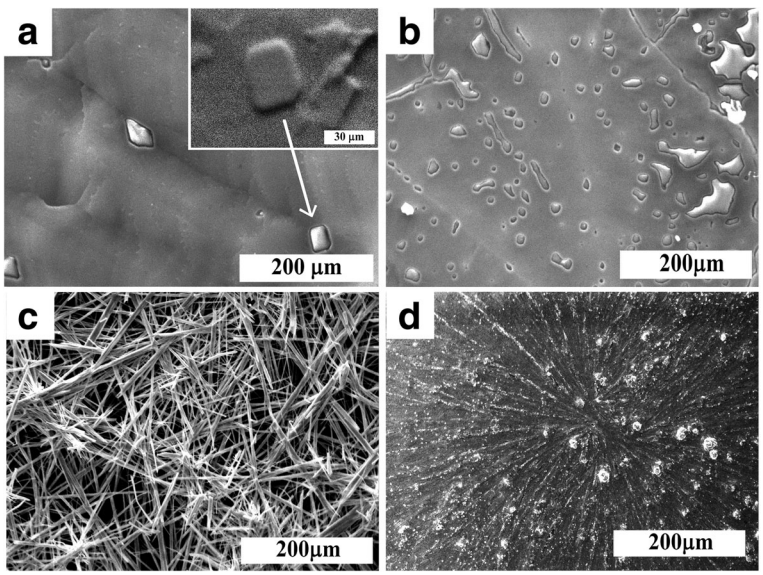

Fig. 2 Images of CH_3NH_3I (**a**, **b**) and PbI_2 (**c**, **d**) films without heating (**a**, **c**) and after thermal treatment at 90 °C (**b**, **d**), deposited on glass substrates. Inset in **a**—increased SEM-BSE image of heterogeneity

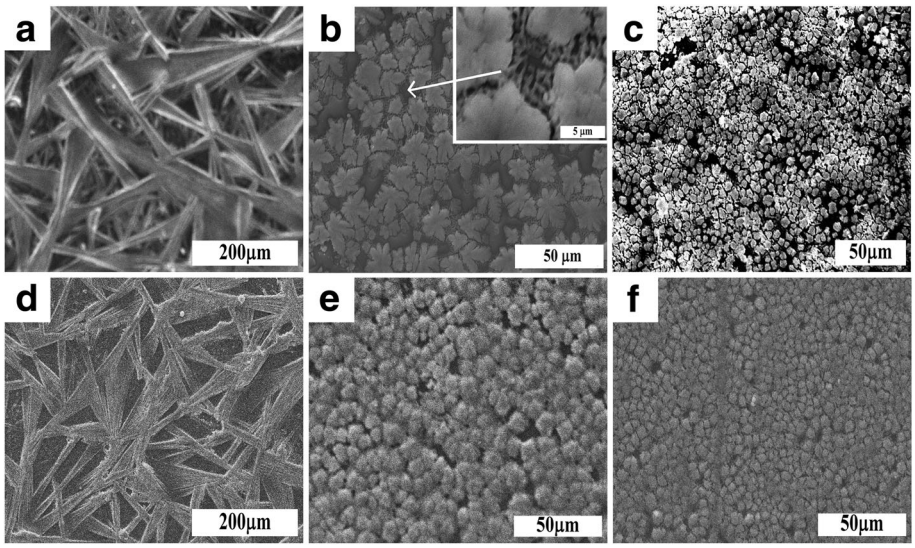

Fig. 3 Images of organic-inorganic perovskites films deposited on glass substrates (**a**-**c**) and FTO/glass (**d**-**f**). Inset in **b**—the enlarged image of the intergrain area

$$\mathrm{PbIz} + \mathrm{CH3NH3I} \overset{70-80^{\circ}C}{\rightarrow} \mathrm{CH3NH3PbI3}. \quad (1)$$

The synthesis of $CH_3NH_3PbI_3$ films was carried out in a glove box, that is why the formation of phases of mono- and dihydrates ($CH_3NH_3PbI_3{\cdot}H_2O$, $(CH_3NH_3)_4PbI_6{\cdot}2H_2O$), which are typical for the synthesis in a humid atmosphere, was not observed (Fig. 4a) [40, 41].

Increasing of the temperatures leads to the appearance of PbI_2 peaks ($2\Theta = 12.8$ °), which can be explained by the partial decomposition of the perovskite. It has been shown that other possible products of the decomposition of perovskite $CH_3NH_3PbI_3$, except for the phase of PbI_2, are CH_3NH_2 and HI [42, 43]. Authors [44] have been shown that in the Fourier-transform infrared spectroscopy (FTIR) spectra of the products, there are bands indicating the presence of a C-I bond. Therefore, the reaction of the decomposition of organic-inorganic perovskite can be written as:

$$\mathrm{CH3NH3PbI3} \overset{>80^{\circ}C}{\rightarrow} \mathrm{PbI2} + \mathrm{CH3I}\uparrow + \mathrm{NH3}\uparrow \quad (2)$$

For the systems, where the starting reagents were in the ratio PbI_2:CH_3NH_3I = 1:2, after evaporation of the solvent, the formation of the additional phase $(CH_3NH_3)_2PbI_4$ has been observed (Fig. 4b). With the increasing of the temperature of heat treatment up to 180 °C, the decreasing of the intensity of this peak have been observed. At 180 °C, the resulting films were single-phase. The scheme of the reaction of formation of perovskite, where the starting reagents were taken in the ratios PbI_2:CH_3NH_3I = 1:2, can be written as:

$$\mathrm{PbI_2} + 2\,\mathrm{CH_3NH_3I} \overset{20-120^{\circ}C}{\rightarrow} (\mathrm{CH_3NH_3})_2\mathrm{PbI_4} \overset{>180^{\circ}C}{\rightarrow} \mathrm{CH_3NH_3PbI_3} + \mathrm{CH_3I}\uparrow + \mathrm{NH_3}\uparrow \quad (3)$$

When the starting reagents were in the ratio PbI_2:CH_3NH_3I = 1:3, the intermediate phase $(CH_3NH_3)_3PbI_5$ was formed, as well as a phase $(CH_3NH_3)_2PbI_4$ (Fig. 4c). Intermediate phases $(CH_3NH_3)_3PbI_5$ and $(CH_3NH_3)_2PbI_4$ were described in [44, 45]. With the increasing of the temperature of heat treatment up to 170 °C, a single-phase perovskite structure is formed. The scheme of the reaction of formation of perovskite can be written as:

$$\mathrm{PbI_2} + 3\,\mathrm{CH_3NH_3I} \overset{20-120^{\circ}C}{\rightarrow} (\mathrm{CH_3NH_3})_3\mathrm{PbI_5} \overset{>120^{\circ}C}{\rightarrow} (\mathrm{CH_3NH_3})_2\mathrm{PbI_4} + \mathrm{CH_3I}\uparrow + \mathrm{NH_3}\uparrow \overset{>170^{\circ}C}{\rightarrow} \mathrm{CH_3NH_3PbI_3} + \mathrm{CH_3I}\uparrow + \mathrm{NH_3}\uparrow \quad (4)$$

With the increase of the temperature of the heat treatment up to 180 °C, thermal decomposition of perovskite in accordance with the chemical reaction (2), has been observed.

It is known that the perovskites of $CH_3NH_3PbI_3$ can take three different phases: orthorhombic at temperatures below − 111 °C [46], tetragonal in the temperature range from − 110 to 51 °C, and cubic at temperatures above 51 °C [47]. In all of our systems (1:1, 1:2, 1:3), tetragonal symmetry (spatial group I4/mcm), which is confirmed by the splitting of peaks (220)/(004), has been observed (Fig. 5).

Figure 5 shows the XRPD diffraction in a narrow 2Θ range (27–29 °) for peaks (220) and (004), for films which were deposited on glass and FTO/glass substrates. The ratio of the intensities of these peaks depends on a

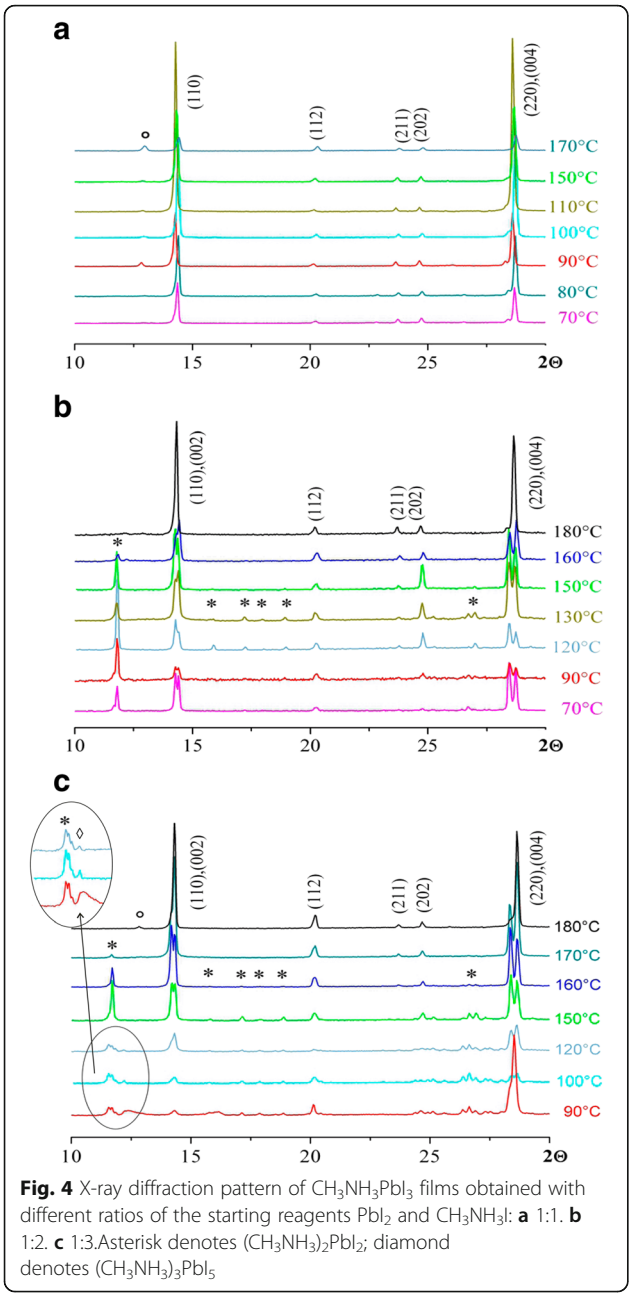

Fig. 4 X-ray diffraction pattern of $CH_3NH_3PbI_3$ films obtained with different ratios of the starting reagents PbI_2 and CH_3NH_3I: **a** 1:1. **b** 1:2. **c** 1:3.Asterisk denotes $(CH_3NH_3)_2PbI_2$; diamond denotes $(CH_3NH_3)_3PbI_5$

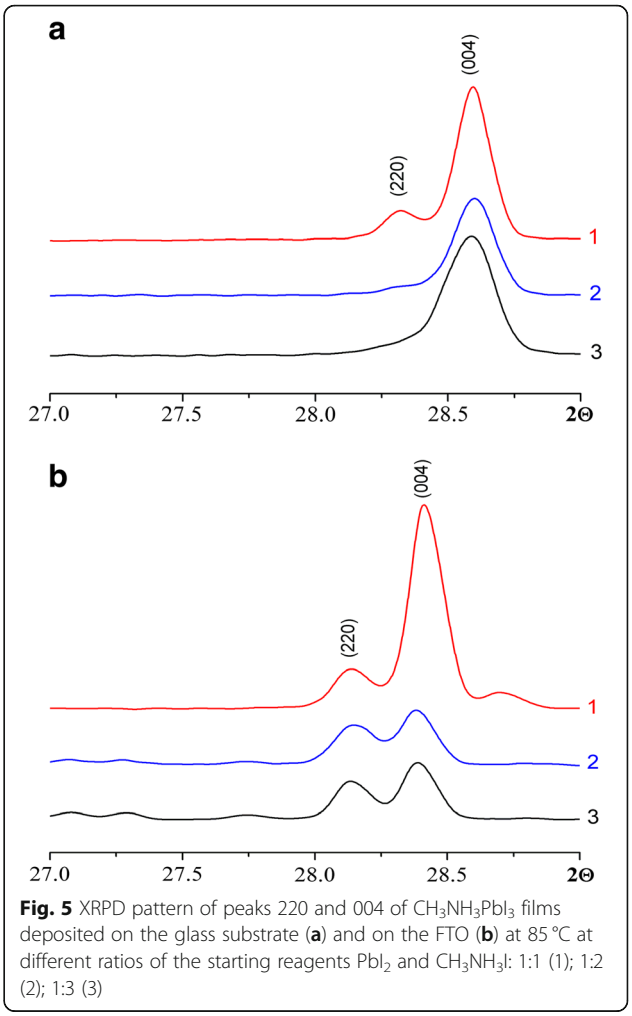

Fig. 5 XRPD pattern of peaks 220 and 004 of $CH_3NH_3PbI_3$ films deposited on the glass substrate (**a**) and on the FTO (**b**) at 85 °C at different ratios of the starting reagents PbI_2 and CH_3NH_3I: 1:1 (1); 1:2 (2); 1:3 (3)

number of factors: chemical composition, occupancy of positions in the structure, and anisotropy of the shape of particles. Previously, we have shown that independent on the ratio of the initial components (CH_3NH_3I:PbI_2 = 1:1, 1:2, 1:3), the ratio between the content of lead and iodine in the films remains unchanged [20]. As has been shown by the calculations, the greatest contribution to the intensity gives the heaviest element—lead (in the ratio 1:2). But for a sample synthesized at a ratio of the starting reagents 1:1, the ratio of the intensities of the peaks is significantly greater than in case of system 1:2. Such a significant difference in the intensity of the peaks (220) and (004) could be explained only by the anisotropy of the particle shape, which is consistent with the data of electron microscopy (Fig. 3). Suitably, the shape of the particles for the sample PbI_2:CH_3NH_3I = 1:1 deposited on the glass substrate is strongly anisotropic (see Fig. 3a). For samples synthesized at a ratio of the initial reagents 1:2 and 1:3, the ratios of the intensities of the peaks (220) and (004) practically the same, which is consistent with the small anisotropy of the particles or its absence (see Fig. 3 b, c respectively). Similar results are observed for samples, where films are deposited on the FTO/glass substrate.

For a more detailed study of the influence of initial reagents ratio PbI_2:CH_3NH_3I and the temperature of crystallization of the film on the formation of perovskites structure, Raman spectroscopy was carried out.

Figure 6, curve 1 shows Raman spectrum of the $CH_3NH_3PbI_3$ film formed from the solution of the PbI_2 and CH_3NH_3I compounds in the ratio (1:1) in DMF and is registered at a sufficiently small power of exciting laser radiation ($\sim 5 \times 10^2$ W/cm^2). The spectra of $CH_3NH_3PbI_3$

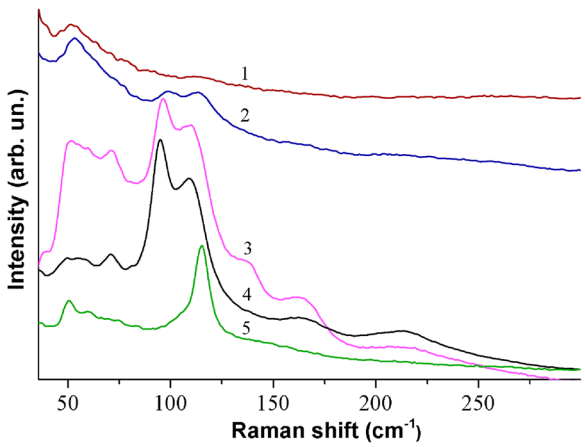

Fig. 6 Raman spectra of $CH_3NH_3PbI_3$ films formed of the 1:1 mixture of PbI_2 and CH_3NH_3I in DMF: directly after deposition on a glass substrate at $T = 90$ °C (1); after irradiation by laser light for 200 s (2); after irradiation for 400 s (3). Raman spectra of films formed from the solution of pure PbI_2 (4) and CH_3NH_3I (5) in DMF. All spectra were obtained with $\lambda_{exc} = 532$ nm at room temperature

films, formed from the solution of PbI_2 and CH_3NH_3I in DMF which are taken in the ratio 1:1, 1:2, and 1:3, are similar and are not shown for the last two films (spectra are shown in Additional file 1). This suggests that despite the different film morphology [32], their structural units are the crystalline lattice of tetragonal perovskite. As noted above, perovskite films are quite sensitive to external factors (moisture, intense X-ray, and laser radiation). When films were irradiated with exciting laser radiation for 200 s, the Raman spectrum changes significantly (Fig. 6, curve 2). A similar change in the spectra occurs when the power density of the exciting laser radiation increases by about five times. With this effect of laser radiation, the $CH_3NH_3PbI_3$ film transforms into a metastable state, which is a transitional state from the perovskite to the PbI_2. Indeed, intense laser radiation can lead to the destruction of chemical bonds in $CH_3NH_3PbI_3$, and to the excitation of the electronic subsystem of individual structural units, which contributes to the formation of a metastable structure. In particular, such a state may be the result of the intercalation of the compound formed due to the partial destruction of the perovskite into PbI_2 [44]. The change in the form of Raman spectra of films in such a metastable state is observed directly in the process of their measurements. In particular, after an additional irradiation of the film by laser radiation during 200 s, the Raman spectrum has significantly changed (Fig. 6, curve 2). In Fig. 6, for comparison, the spectra of films formed by the deposition of DMF solution with PbI_2 (curve 4) and CH_3NH_3I (curve 5) compounds are also given. Further increase in the time of irradiation of the $CH_3NH_3PbI_3$film by laser radiation with the same power leads to the complete destruction of $CH_3NH_3PbI_3$. As a result, the spectrum is similar to curve 4, in Fig. 3, which corresponds to the vibrational spectra of the PbI_2 compound. It should be noted that the destruction of the $CH_3NH_3PbI_3$ perovskite during its interaction with moisture is much slower [48].

The results of X-ray diffraction analysis showed that when the ratio of the initial reagents PbI_2:CH_3NH_3I = 1:2 and 1:3, the formation of the perovskite structure occurs through intermediates $(CH_3NH_3)_3PbI_5$ and $(CH_3NH_3)_2PbI_4$. In Raman spectra, it is difficult to detect these compounds, since the frequencies of the vibrational modes of $CH_3NH_3PbI_3$, $(CH_3NH_3)_3PbI_5$ and $(CH_3NH_3)_2PbI_4$ in the low-frequency region of the spectrum are quite close [49].

We also carried out Raman studies of perovskite films formed from solutions of PbI_2 and CH_3NH_3I compounds (1:3) in DMF, which were annealed in the temperature range from 100 to 180 °C (Fig. 7). The spectra of films that were treated at temperatures up to 180 °C are quite similar to the spectrum 1, which is shown in Fig. 6. However, the Raman spectrum of the film that was treated at $T = 180$ °C already corresponds to the spectrum of the metastable phase (curve 3 in Fig. 6). These results correlate with the data of X-ray diffraction analysis.

Conclusions

Therefore, the possibility to control morphology, structural, and optical properties of $CH_3NH_3PbI_3$ films by variation of the ratio of initial compounds, of PbI_2 and CH_3NH_3I in DMF solvent, was found. X-ray diffraction analysis has shown that the formation of the perovskite structure with the ratio of the initial reagents PbI_2: CH_3NH_3I = 1:1 occurs at 70–80 °C, and with the increase of the temperature of thermal treatment to 120 °C, the thermal destruction of the perovskite begins. When the

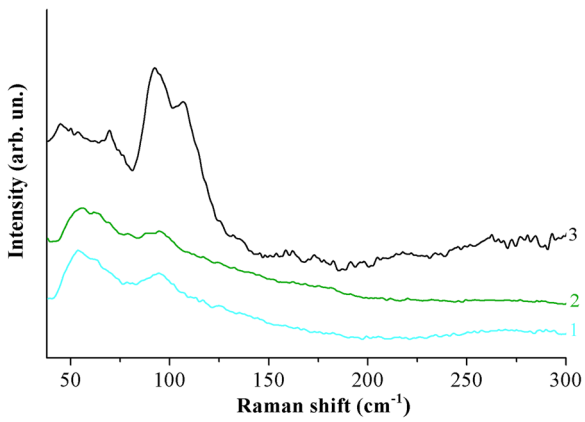

Fig. 7 Raman spectra of the films formed of the solution of PbI_2 and CH_3NH_3I compounds in DMF in the ratio (1:3) at temperatures of 100 (1), 150 (2), and 180 °C (3). All spectra were obtained with λ_{exc} = 532 nm at room temperature

ratio of the starting reagents PbI_2: CH_3NH_3I = 1:2, the formation of the perovskite structure occurs through the intermediate compound $(CH_3NH_3)_2PbI_4$, and when the ratio is 1:3—$(CH_3NH_3)_3PbI_5$ and $(CH_3NH_3)_2PbI_4$. Independent on the ratio of the initial components (CH_3NH_3I:PbI_2), the ratio between the content of lead and iodine in the films remains unchanged, that is why a significant difference in the film properties could be explained by the anisotropy of the particle shape, which is consistent with the data of electron microscopy, as well as with X-ray diffractometry (change in the ration of peaks (220) and (004) intensity). By using Raman spectroscopy, it was shown that films are sensitive to laser radiation, which leads to destruction, the final product of which is PbI_2. When illuminated with laser radiation with low power density, they may be in a metastable state for some time, which is a transition from perovskite to PbI_2.

Additional file

Additional file 1: Figure S1. UV-vis absorption spectra of solutions: 1 – PbI_2; 2 – PbI_2 and CH_3NH_3I (1:1); 3 – PbI_2 and CH_3NH_3I (1:2); 4 – PbI_2 and CH_3NH_3I (1:3) in DMF. Figure S2 Raman spectra of the films formed of the solution of PbI_2 and CH_3NH_3I in DMF in the ratio 1:1 (1); 1:2 (2); and 1:3 (3) at 90 °C. All spectra were recorded with λ_{exc} = 532 nm at room temperature. Figure S3 (a) Back-scattered electrons (BSE) images of heterogeneity on the surface of CH_3NH_3I films prepared at room temperature (no heating). (b) Energy-dispersive X-ray (EDX) spectra of the region selected within the heterogeneity asea (Selected Area 1) and outside of heterogeneity (Selected Area 2). (c) Cross-section of the film CH_3NH_3I on the surface of the glass in the area of heterogeneity. (DOCX 894 kb)

Abbreviations

BSE: Backscattering electrons; CCD: Charge-coupled device; DMF: Dimethylformamide, C_3H_7NO; EDX: Energy-dispersive X-ray spectroscopy; FTIR: Fourier-transform infrared spectroscopy; FTO: Fluorine-doped tin oxide; MAI: Methylammonium iodide; $MAPbI_3$: Methylammonium lead iodide perovskites, $CH_3NH_3PbI_3$; $MAPbI_{3-x}Cl_x$: Methylammonium lead iodide chloride perovskites, $CH_3NH_3PbI_{2.98}Cl_{0.02}$; OIP: Organic-inorganic perovskites; PCE: Power conversion efficiencies; XRPD: X-ray powder diffractometry

Acknowledgements

The work was carried out with the financial support from the targeted research program of the Ukrainian National Academy of Sciences "Fundamental Issues of Creation of Novel Nanomaterials and Nanotechnologies" (Novel Nanomaterials).

Funding

The authors would like to thank the Ukrainian National Academy of Sciences for providing the research grant (34/18-H) to support this work.

Availability of data and materials

The datasets generated and/or analyzed during the current study are available from the corresponding author on reasonable request.

Authors' contributions

AB supervised the work and finalized the manuscript. SK performed the X-ray powder diffraction. OV performed SEM, and EDX investigations and took part in analyzing the obtained results. PT synthesized the films of hybrid organic-inorganic halides with perovskite structure. VY carried out an analysis of the Raman spectra and their interpretation. OH measured the Raman spectra. AG, SK, OV, PT, VY, and OH contributed on the drafting and revision of the manuscript. All authors read and approved the final manuscript.

Competing interests

The authors declare that they have no competing interests.

Publisher's Note

Author details

[1]V.I. Vernadskii Institute of General and Inorganic Chemistry of the NAS of Ukraine, Kyiv, Ukraine. [2]V. Lashkaryov Institute of Semiconductor Physics, NAS of Ukraine, Kyiv, Ukraine.

Received: 15 October 2018 Accepted: 18 December 2018
Published online: 05 January 2019

References

1. Chu S, Cui Y, Liu N (2017) The path towards sustainable energy. Nature materials. 16(1):16
2. Lee TD, Ebong AU. A review of thin film solar cell technologies and challenges. Renewable and Sustainable Energy Reviews. 2017;70:1286–97
3. . Simbolotti G, Taylor M. Photovoltaic Solar Power IEA-ETSAP and IRENA Technology Brief E11. 2013; (January):[1–11 pp.]. Available from: https://iea-etsap.org/E-TechDS/PDF/E11IR_PV_GSMT_Jan2013_final_GSOK.pdf
4. Sharma S, Jain KK, Sharma A (2015) Solar cells: in research and applications—a review. Materials Sciences and Applications. 6(12):1145
5. Wang C, Zhang C, Wang S, Liu G, Xia H, Tong S et al (2018) Low-temperature processed, efficient, and highly reproducible cesium-doped triple cation perovskite planar heterojunction solar cells. Solar RRL 2(2): 1700209
6. Gu X, Wang Y, Zhang T, Liu D, Zhang R, Zhang P et al (2017) Enhanced electronic transport in Fe3+-doped TiO2 for high efficiency perovskite solar cells. J Mater Chem C 5(41):10754–10760
7. Kojima A, Teshima K, Shirai Y, Miyasaka T (2009) Organometal halide perovskites as visible-light sensitizers for photovoltaic cells. J Am Chem Soc 131(17):6050–6051
8. Yang WS, Park B-W, Jung EH, Jeon NJ, Kim YC, Lee DU et al (2017) Iodide management in formamidinium-lead-halide–based perovskite layers for efficient solar cells. Science 356(6345):1376–1379
9. Chart (2018) Best research-cell efficiencies. In: National Renewable Energy Laboratory Available from: https://www.nrel.gov/pv/assets/pdfs/pv-efficiency-chart.20181221.pdf
10. Jeon NJ, Na H, Jung EH, Yang T-Y, Lee YG, Kim G et al (2018) A fluorene-terminated hole-transporting material for highly efficient and stable perovskite solar cells. Nat Energy 3(8):682–689
11. Zhang T, Wu J, Zhang P, Ahmad W, Wang Y, Alqahtani M et al (2018) High speed and stable solution-processed triple cation perovskite photodetectors. Advanced Optical Materials:1701341
12. . Wang Y, Wu J, Zhang P, Liu D, Zhang T, Ji L, et al. Stitching triple cation perovskite by a mixed anti-solvent process for high performance perovskite solar cells. Nano Energy. 2017;39:616–25
13. Sharenko A, Toney MF (2015) Relationships between lead halide perovskite thin-film fabrication, morphology, and performance in solar cells. J Am Chem Soc 138(2):463–470
14. Xiong J, Yang B, Cao C, Wu R, Huang Y, Sun J et al (2016) Interface degradation of perovskite solar cells and its modification using an annealing-free TiO2 NPs layer. Org Electron. 30:30–35
15. Peng Y, Cheng Y, Wang C, Zhang C, Xia H, Huang K et al (2018) Fully doctor-bladed planar heterojunction perovskite solar cells under ambient condition. Org Electron. 58:153–158
16. Cao C, Zhang C, Yang J, Sun J, Pang S, Wu H et al (2016) Iodine and chlorine element evolution in CH3NH3PbI3–xClx thin films for highly efficient planar heterojunction perovskite solar cells. Chem Mater 28(8): 2742–2749
17. V'yunov O, Belous A, Kobylianska S, Kovalenko L (2018) Impedance analysis of thin films of organic-inorganic perovskites CH3NH3PbI3 with control of microstructure. Nanoscale Research Letters. 13(1):98

18. Yin WJ, Shi T, Yan Y (2014) Unique properties of halide perovskites as possible origins of the superior solar cell performance. Adv Mater 26(27): 4653–4658
19. Chen Q, De Marco N, Yang YM, Song T-B, Chen C-C, Zhao H et al (2015) Under the spotlight: the organic–inorganic hybrid halide perovskite for optoelectronic applications. Nano Today 10(3):355–396
20. Sutton RJ, Eperon GE, Miranda L, Parrott ES, Kamino BA, Patel JB et al (2016) Bandgap-tunable cesium lead halide perovskites with high thermal stability for efficient solar cells. Advanced Energy Materials. 6(8):1502458
21. Eperon GE, Stranks SD, Menelaou C, Johnston MB, Herz LM, Snaith HJ (2014) Formamidinium lead trihalide: a broadly tunable perovskite for efficient planar heterojunction solar cells. Energy Environ Sci 7(3):982–988
22. Conings B, Drijkoningen J, Gauquelin N, Babayigit A, D'Haen J, D'Olieslaeger L et al (2015) Intrinsic thermal instability of methylammonium lead trihalide perovskite. Advanced Energy Materials. 5(15):1500477
23. You J, Meng L, Song T-B, Guo T-F, Yang Y, Chang W-H et al (2015) Improved air stability of perovskite solar cells via solution-processed metal oxide transport layers. Nat Nanotechnol 11(1):75–81
24. Han Y, Meyer S, Dkhissi Y, Weber K, Pringle JM, Bach U et al (2015) Degradation observations of encapsulated planar CH3NH3PbI3 perovskite solar cells at high temperatures and humidity. J Mater Chem A 3(15):8139–8147
25. . Dualeh DA, Tétreault N, Moehl T, Gao P, Nazeeruddin MK, Grätzel M. Effect of annealing temperature on film morphology of organic–inorganic hybrid pervoskite solid-state solar cells. Adv Funct Mater 2014;24(21):3250–3258
26. Leguy AIM, Hu Y, Campoy-Quiles M, Alonso MI, Weber OJ, Azarhoosh P et al (2015) Reversible hydration of CH3NH3PbI3 in films, single crystals, and solar cells. Chem Mater 27(9):3397–3407
27. Kalaiselvi C, Muthukumarasamy N, Velauthapillai D, Kang M, Senthil T (2018) Importance of halide perovskites for next generation solar cells–a review. Mater Lett. 219:198–200
28. Ansari MIH, Qurashi A, Nazeeruddin MK (2018) Frontiers, opportunities, and challenges in perovskite solar cells: A critical review. Journal of Photochemistry and Photobiology C: Photochemistry Reviews. 35:1–24
29. Qiu L, Ono LK, Qi Y (2017) Advances and challenges to the commercialization of organic–inorganic halide perovskite solar cell technology. Materials Today Energy. 7:169–189
30. Manser JS, Saidaminov MI, Christians JA, Bakr OM, Kamat PV (2016) Making and breaking of lead halide perovskites. Acc Chem Res 49(2):330–338
31. Li S, Zhang P, Wang Y, Sarvari H, Liu D, Wu J et al (2017) Interface engineering of high efficiency perovskite solar cells based on ZnO nanorods using atomic layer deposition. Nano Res 10(3):1092–1103
32. Belous AG, V'yunov OI, Kobylyanskaya SD, Ishchenko AA, Kulinich AV (2018) Influence of synthesis conditions on the morphology and spectral-luminescent properties of films of organic-inorganic perovskite CH3NH3PbI2.98Cl0.02. Russ J Gen Chem. 88(1):114–119
33. Liu J, Lin J, Xue Q, Ye Q, He X, Ouyang L et al (2016) Growth and evolution of solution-processed CH3NH3PbI3-xClx layer for highly efficient planar-heterojunction perovskite solar cells. J Power Sources. 301:242–250
34. Qiu J, Qiu Y, Yan K, Zhong M, Mu C, Yan H et al (2013) All-solid-state hybrid solar cells based on a new organometal halide perovskite sensitizer and one-dimensional TiO2 nanowire arrays. Nanoscale 5(8):3245–3248
35. Niemann RG, Kontos AG, Palles D, Kamitsos EI, Kaltzoglou A, Brivio F et al (2016) Halogen effects on ordering and bonding of CH3NH3+ in CH3NH3PbX3 (X = Cl, Br, I) hybrid perovskites: a vibrational spectroscopic study. J Phys Chem C 120(5):2509–2519
36. Dai ZR, Pan ZW, Wang ZL (2003) Novel nanostructures of functional oxides synthesized by thermal evaporation. Adv Funct Mater 13(1):9–24
37. Kurilo I, Rybak O (2002) Effect of growth conditions on the morphology and structural perfection of vapor-grown PbI2 crystals. Inorg Mater 38(3):288–291
38. Liu D, Zhou W, Tang H, Fu P, Ning Z. Supersaturation controlled growth of MAFAPbI3 perovskite film for high efficiency solar cells. Science China Chemistry. 2018:1–7
39. Fu F, Kranz L, Yoon S, Löckinger J, Jäger T, Perrenoud J et al (2015) Controlled growth of PbI2 nanoplates for rapid preparation of CH3NH3PbI3 in planar perovskite solar cells. Phys Status Solidi A 212(12):2708–2717
40. Kye Y-H, Yu C-J, Jong U-G, Chen Y, Walsh A (2018) Critical role of water in defect aggregation and chemical degradation of perovskite solar cells. J Phys Chem Lett 9(9):2196–2201
41. Vincent BR, Robertson KN, Cameron TS, Knop O (1987) Alkylammonium lead halides. Pt 1. Isolated PbI64− ions in (CH3NH3)4PbI6·2H2O. Can J Chem. 65(5):1042–1046
42. Rajagopal A, Yao K, Jen AKY (2018) Toward perovskite solar cell commercialization: a perspective and research roadmap based on interfacial engineering. Adv Mater.:1800455
43. Chen X, Cao H, Yu H, Zhu H, Zhou H, Yang L et al (2016) Large-area, high-quality organic–inorganic hybrid perovskite thin films via a controlled vapor–solid reaction. J Mater Chem A 4(23):9124–9132
44. Roghabadi FA, Ahmadi V, Aghmiuni KO (2017) Organic–inorganic halide perovskite formation: in situ dissociation of cation halide and metal halide complexes during crystal formation. J Phys Chem C 121(25):13532–13538
45. Petrov AA, Sokolova IP, Belich NA, Peters GS, Dorovatovskii PV, Zubavichus YV et al (2017) Crystal structure of DMF-intermediate phases uncovers the link between CH3NH3PbI3 morphology and precursor stoichiometry. J Phys Chem C 121(38):20739–20743
46. Poglitsch A, Weber D (1987) Dynamic disorder in methylammoniumtrihalogenoplumbates (II) observed by millimeter-wave spectroscopy. J Chem Phys 87(11):6373–6378
47. Kawamura Y, Mashiyama H, Hasebe K (2002) Structural study on cubic-tetragonal transition of CH3NH3PbI3. J Phys Soc Jpn 71(7):1694–1697
48. Segovia R, Qu G, Peng M, Sun X, Shi H, Gao B (2018) Evolution of photoluminescence, Raman, and structure of CH3NH3PbI3 perovskite microwires under humidity exposure. Nanoscale research letters. 13(1):79
49. Koh TM, Thirumal K, Soo HS, Mathews N (2016) Multidimensional perovskites: a mixed cation approach towards ambient stable and tunable perovskite photovoltaics. ChemSusChem 9(18):2541–2558